A Theoretical Investigation of Single-Molecule Fluorescence Detection on Thin Metallic Layers

Jörg Enderlein
Institute of Analytical Chemistry, Chemo- and Biosensors, University of Regensburg, PF 10 10 42, D-93040 Regensburg, Germany

ABSTRACT In the present paper, the excitation and detection of single-molecule fluorescence over thin metallic films is studied theoretically within the framework of classical electrodynamics. The model takes into account the specific conditions of surface plasmon-assisted optical excitation, fluorescence quenching by the metal film, and detection geometry. Extensive numerical results are presented for gold, silver, and aluminum films, showing the detectable fluorescence intensities and their dependence on film thickness and the fluorescent molecule's position under optimal excitation conditions.

INTRODUCTION

In recent years, the detection and spectroscopy of individual fluorescing molecules on surfaces has seen a tremendous development (see e.g., Basché et al., 1997). The commonly used techniques for detecting single molecules on surfaces are wide-field, confocal, and near-field microscopy. The molecules are excited by laser light, that is either focused by an appropriate microscope objective onto the surface, or delivered by a tapered optical fiber tip. In all cases, collection of fluorescence is done through a light-collecting microscope objective, either from above the supporting surface, or through the transparent support itself.

Usually, the molecules to be studied are immobilized on a transparent dielectric (glass or fused silica), which has, from an electrodynamic point of view, rather moderate effects on their emission properties. For example, if molecules are adsorbed on a glass surface (refractive index 1.5) from a watery solution (refractive index 1.33), classical electrodynamics predicts that their radiative transition rate is enhanced by a factor between 1.07 and 1.33, depending on the molecules' emission dipole orientation with respect to the glass surface. A useful side effect is that, when detecting through the transparent glass support, between 68 and 77% of the fluorescence is emitted toward the glass side, thus enhancing the light-collection efficiency (Enderlein et al., 1999).

However, in many biomolecular techniques such as the self-assembly and self-organization of layers of lipids and proteins, metal surfaces play a unique role. For example, a widely used technique is the self-assembly of monolayers of thiol molecules by covalent bonding of their sulfur groups on metals such as gold or silver. For metal surfaces, the fluorescence-emission properties of immobilized molecules differ significantly from those of molecules placed on a transparent dielectric with negligible optical absorption (Chance et al., 1978). For a metal with large complex values in its refractive index, the strong electromagnetic coupling between the fluorescing molecule and the metal leads to a strong energy transfer from the molecule to the metal, resulting in a nearly complete fluorescence quenching. Thus, sensitive fluorescence detection of a few or single molecules on metals seems a rather difficult if not impossible task. In contrast, when considering the fluorescence detection of molecules on thin metallic films, one has not only the disadvantage of strong fluorescence quenching, but also the possibility of enhancing the fluorescence excitation by using the enhanced electromagnetic field of surface plasmons. A further, often underestimated effect, is the very strong dependence of the fluorescence quenching on the molecule's distance from the surface. Shifting a molecule only a few nanometers away may lead to an emission enhancement by orders of magnitude. Finally, the strong energy transfer from the excited molecule to the metal films dramatically shortens the lifetime of the excited state, thus significantly increasing the number of excitation cycles a molecule can survive until photobleaching occurs (Enderlein, 1999).

Recently, Yokota et al. (1998) demonstrated experimentally the detection of single molecules of tetramethylrhodamine (TMR) and Cy5 at a distance of a few nanometers (~7–25) from thin metallic films of gold, silver, and aluminum. They excited the fluorescence via surface plasmons generated in a Kretschmann–Raether configuration, and detected the fluorescence through a water-immersion microscope objective (see Fig. 1). The aim of the present paper is to give, within the framework of classical electrodynamics, a detailed theoretical study of single molecule fluorescence detection in such an experimental configuration, taking into account the special conditions of surface plasmon-supported excitation, fluorescence quenching, and light-collection geometry. We report extensive numerical results for gold, silver, and aluminum, showing the dependence of the fluorescence-detection efficiency on film thickness, incidence

Received for publication 19 May 1999 and in final form 21 December 1999.

Address reprint requests to Jörg Enderlein, Institute of Analytical Chemistry, Chemo- and Bio-Sensors, University of Regensburg, Universitätsstr. 31, D-93053 Regensburg, Germany. Tel.: +49-941-943-4048; Fax: +49-941-943-4491; E-mail: joerg.enderlein@chemie.uni-regensburg.de.

0006-3495/00/04/2151/08 $2.00

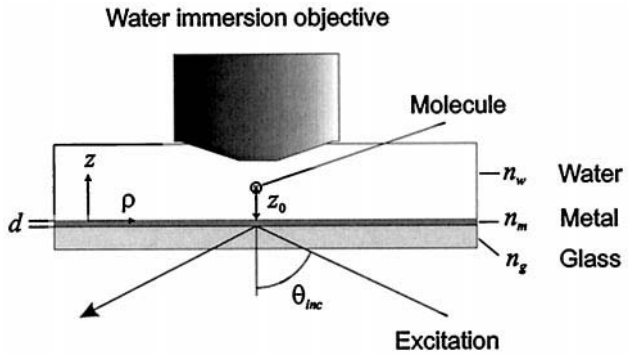

FIGURE 1 Schematic of the experimental set-up studied in the present paper. Fluorescence excitation is performed in the evanescent electromagnetic field above the metal film, which is produced by an incident plane wave from below with incidence angle θ_{inc}. The fluorescing molecule is positioned within a water solution at a distance d from the metal surface, and the emanating fluorescence is detected by a water-immersion objective.

angle of excitation light, and the molecules' distance from the surface.

THEORY

The experimental set-up studied in this paper is shown in Fig. 1. A thin metal film of thickness d and with complex refractive index n_m is deposited on a glass substrate with refractive index n_g. Above the film, fluorescing molecules are placed at a distance z_0 from the metal's surface within a liquid environment with refractive index n_w. A plane wave of light is directed from below (the glass side) onto the metal film under an incidence angle θ_{inc}. Because we are interested in surface plasmon effects, we consider, here, only plane waves with p-polarization, that is, with an electric field vector within the plane of incidence. The molecule's fluorescence is detected from above (water side) through a water-immersion objective with numerical aperture NA.

For a plane wave with incidence angle θ_{inc} hitting the metal film from below, the exciting electric field above the metal surface is given by (Born and Wolf, 1989)

$$T_p = \frac{t_p^{gm}\, t_p^{mw}}{1 + r_p^{gm}\, r_p^{mw} \exp(2il_m d)}, \qquad (1)$$

where l_m stands for $k_0[n_m^2 - n_g^2 + \cos^2\theta_{inc}]^{1/2}$ with k_0 being the length of the vacuum wave vector, and the t_p^{ab} and r_p^{ab} are the Fresnel transmission and reflection coefficients for a single interface between medium a and b.

For finding the amount of fluorescence quenching by the metal layer, we will proceed by the following steps. The fluorescing molecule will be considered as an oscillating electric dipole. The electromagnetic field emitted by this dipole is interacting with the metal film/glass environment, creating a back-reaction field $E_R(\vec{r})$. This back-reaction field may enhance or dampen the dipole's emission, thus changing the transition rate of the molecule from the excited state to the ground state. For obtaining the probability that a photon emitted by the molecule is collected by the microscope objective, the electromagnetic energy flux emitted into the objective must be calculated and then divided by the total amount of energy emitted, taking into account the energy flowing through the water–metal interface. In this theoretical approach, the medium surrounding the molecule is considered to be electrodynamically homogeneous and completely characterized by its refractive index. Any possible repolarization of the solvent during the molecule's excited state lifetime is implicitly accounted for by choosing the appropriately shifted emission wavelength of the molecule (Lippert effect), but does not have a direct influence of the emission dynamics, because changes of solvent polarization occur on a much slower time scale (picosecond) than the process of photon emission (femtosecond). Also, the presence of free ions in solutions (as in salt buffers) does not have a direct influence on the emission dynamics except of possibly changing the refractive index. One has to bear in mind that any process much slower than the emission of a photon by the molecule can be dealt with as quasi-static, and its influence should be accounted for by the refractive index of the solution, which can be considered to be constant during the emission process.

Thus, the first goal of the following paragraphs will be to find an expression of the electromagnetic field of the emitting dipole over the metal film/glass sandwich. In what follows, an $\exp(-i\omega t)$ time dependence of the electromagnetic field and the dipole strength is assumed. The starting point for our further considerations is the so-called Weyl representation of the electric field amplitude $E_D(\vec{r})$ of an oscillating dipole with amplitude $\vec{p}$ at position $\vec{r}_0$ within a homogeneous environment with refractive index n_w (Girard and Dereux, 1994):

$$\vec{E}_D(\vec{r}) = \frac{i}{2\pi n_w^2} \int \frac{d^2\vec{q}}{l_w} [k_w^2\, \vec{p} - \vec{k}_w^{\pm}(\vec{k}_w^{\pm} \cdot \vec{p})] \times \exp(i\vec{q} \cdot (\vec{\rho} - \vec{\rho}_0) + il_w|z - z_0|), \qquad (2)$$

where we used the abbreviations $\vec{r} = (\vec{\rho}, z)$, $\vec{r}_0 = (\vec{\rho}_0, z_0)$, $\vec{k}_w^{\pm} = (\vec{q}, \pm l_w)$, $l_w = \sqrt{k_w^2 - q^2}$, $k_w \equiv |\vec{k}_w^{\pm}|$, and $\int d^2\vec{q}$ denotes integration over the whole two-dimensional $\vec{q}$-space. The geometry of this plane wave representation of the electric field is depicted in Fig. 2. The plus sign in the above equation applies if $z - z_0 > 0$, the minus sign if $z - z_0 < 0$. The vectors $\vec{\rho}$, $\vec{\rho}_0$, and $\vec{q}$ are the vector parts of $\vec{r}$, $\vec{r}_0$, and $\vec{k}_w^{\pm}$ perpendicular to the z-direction. The value of l_w is assumed to lie always within the first quadrant of the complex plane.

For obtaining the back-reaction field, every plane wave in this representation has to be reflected by the metal film/glass substrate according to Fresnel's formulas. For apply-

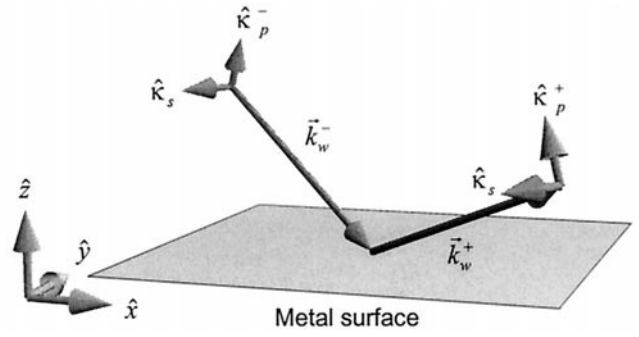

FIGURE 2 Geometry of the plane wave reflection at the water–metal boundary.

ing the last, one has first to separate the *p*- and *s*-polarized components in Eq. 1, which can be done by exploiting the identity

$$k_w^2\,\hat{I} - \vec{k}_w^{\pm} \otimes \vec{k}_w^{\pm} = k_w^2(\hat{\kappa}_p^{\pm} \otimes \hat{\kappa}_p^{\pm} + \hat{\kappa}_s \otimes \hat{\kappa}_s), \qquad (3)$$

where $\hat{I}$ is the unit matrix, the symbol $\otimes$ denotes tensorial multiplication, $(\vec{a} \otimes \vec{b})_{jk} = a_j b_k$, and the unit vectors $\hat{\kappa}_p^{\pm}$ and $\hat{\kappa}_s$ are given by

$$\hat{\kappa}_p^{\pm} = \frac{1}{k_w}(\mp l_w \hat{q}, q), \qquad \hat{\kappa}_s = (\hat{z} \times \hat{q}, 0), \qquad (4)$$

where $\hat{q}$ and $\hat{z}$ are unit vectors along $\vec{q}$ and the *z*-axis, respectively (see Fig. 2). The unit vectors $\hat{\kappa}_p^{\pm}$ and $\hat{\kappa}_s$ are the electric field polarization unit vectors of *p*- and *s*-waves with respect to the plane $z = 0$ (see Fig. 2). Thus, Eq. 2 can be rewritten as

$$\vec{E}_D(\vec{r}) = \frac{ik_0^2}{2\pi}\int \frac{d^2\vec{q}}{l_w}\,[\hat{\kappa}_p^{\pm}(\hat{\kappa}_p^{\pm}\cdot\vec{p}) + \hat{\kappa}_s(\hat{\kappa}_s\cdot\vec{p})]$$

$$\times \exp(i\vec{q}\cdot(\vec{\rho} - \vec{\rho}_0) + il_w|z - z_0|). \qquad (5)$$

The total reflection coefficients at the water–metal interface are given by (Born and Wolf, 1989),

$$R_{p,s} = \frac{r_{p,s}^{wm} + r_{p,s}^{mg}\exp(2il_m d)}{1 + r_{p,s}^{wm}\,r_{p,s}^{mg}\exp(2il_m d)}, \qquad (6)$$

where the subscripts refer to *p*- and *s*-polarization, the $r_{p,s}^{wm}$ and $r_{p,s}^{mg}$ are the Fresnel reflection coefficients for the single water-to-metal and metal-to-glass transition, and l_m is, here, the abbreviation for $l_m = [(n_m^2 - n_w^2)k_0^2 + l_w^2]^{1/2}$. Now, the back-reaction field $\vec{E}_R$ is found by reflecting every plane wave in Eq. 5 according to Eq. 6:

$$\vec{E}_R(\vec{r}) = \frac{ik_0^2}{2\pi}\int \frac{d^2\vec{q}}{l_w}\,[\hat{\kappa}_p^{+} R_p(\hat{\kappa}_p^{-}\cdot\vec{p}) + \hat{\kappa}_s R_s(\hat{\kappa}_s\cdot\vec{p})]$$

$$\times \exp(i\vec{q}\cdot(\vec{\rho} - \vec{\rho}_0) + il_w|z - z_0|). \qquad (7)$$

Next, we will derive an expression for the angular distribution of the emission intensity into the water half-space. The energy flux of a plane wave with electric field amplitude $E_0 \exp i\vec{k}\cdot\vec{r}$ in water along its direction of propagation is given by the modulus of the Poynting vector, $S = cn_w|E_0^2|/8\pi$, where *c* is the vacuum speed of light. Thus, after inspecting the total electric field amplitude of the emitting dipole as given by the sum of Eq. 5 and Eq. 7, one may expect the following expression for the energy flux of the dipole emission into the solid angle element $d\Omega$ at a direction with polar angle $\theta = \arctan q/l_w$ and azimuthal angle $\phi = \arctan q_y/q_x$:

$$\frac{dS_+}{d\Omega} = Cn_w\left|\frac{k_0^3\,n_w}{2\pi}\right|^2 |\hat{\kappa}_p^{+}(\hat{\kappa}_p^{+}\cdot\vec{p})$$

$$+ \hat{\kappa}_p^{+} R_p(\hat{\kappa}_p^{-}\cdot\vec{p}) + \hat{\kappa}_s(1 + R_s)(\hat{\kappa}_s\cdot\vec{p})|^2, \qquad (8)$$

where we have taken into account that $l_w = k_w \cos\theta$ and $d\Omega = \sin\theta d\theta d\phi = d^2\vec{q}/k_w l_w$. The subscript at S_+ indicates that we are dealing with the emission into the positive half space ($z > 0$). The constant *C* can be found by studying the special case when all dielectric constants are equal, $n_g = n_m = n_w$. Then, $R_p = R_s = 0$, and one finds (see Eq. 3),

$$\frac{dS_+}{d\Omega} = Cn_w\left|\frac{k_0^3\,n_w}{2\pi}\right|^2 [k_w^2 p^2 - (\vec{k}_w^{+}\cdot\vec{p})^2], \qquad (9)$$

which describes the emission of a free dipole if $C = \pi c/2n_w^2 k_0^2$ (Jackson, 1975). Having the angular distribution of emission at hand, the total energy flux into the water half space (S_+^{tot}) and into the microscope objective (S_+^{obj}) are given by

$$S_+^{tot,obj} = \int_0^{\theta_{max}} d\theta \sin\theta \int_0^{2\pi} d\phi\,\frac{dS_+}{d\Omega}, \qquad (10)$$

where θ_{max} equals $\pi/2$ for the complete half space, and $\theta_{max} = \arcsin NA/n_w$ for the microscope objective.

Finally, we need the total energy flux S_- through the water–metal interface. This flux is given by integrating the projection of the Poynting vector along the negative *z*-direction over this interface,

$$S_- = -\frac{c}{8\pi}\,\mathrm{Re}\int_{z=0} dA\hat{z}\cdot\vec{E}\times\vec{B}^*. \qquad (11)$$

Using the results from Eq. 5 and Eq. 7, and taking into account that $k_0\vec{B} = \vec{\nabla}\times\vec{E}$, one finds that

$$S_- = \frac{ck_0^3}{8\pi}\,\mathrm{Re}\int \frac{d^2\vec{q}}{|l_w^*|}\,[l_w(1 - R_p)(1 + R_p^*)|(\hat{\kappa}_p^{-}\cdot\vec{p})^2|$$

$$+ l_w^*(1 + R_s)(1 - R_s^*)|(\hat{\kappa}_s\cdot\vec{p})^2|]\exp[-2\,\mathrm{Im}(l_w)z_0], \qquad (12)$$

TABLE 1 Values of the complex refractive indices of gold, silver, and aluminum at the different wavelengths used in the present work.

	Wavelength (nm)			
Metal	514	580	633	670
Gold	$0.71 + i1.96$	$0.29 + i2.69$	$0.20 + i3.26$	$0.17 + i3.61$
Silver	$0.14 + i2.91$	$0.15 + i3.42$	$0.16 + i3.80$	$0.16 + i4.07$
Aluminum	$0.84 + i6.02$	$1.07 + i6.71$	$1.27 + i7.28$	$1.45 + i7.70$

where * denotes complex conjugation.

Having the expressions for the energy flux into the water half space S_+^{tot}, the microscope objective S_+^{obj}, and through the water–metal interface S_-, the probability that the microscope objective will see a photon emitted by the molecule is given by the ratio $S_+^{\text{obj}}/(S_+^{\text{tot}} + S_-)$. For obtaining a final expression for the fluorescence emission intensity observed through the microscope objective, the results for the fluorescence excitation and detection of the preceding paragraphs have to be combined. This needs some additional information about the molecule's dipole orientation during excitation and fluorescence emission. Here, we will only consider the simple and experimentally most interesting case that the characteristic time of rotational diffusion of the molecule is much faster than the fluorescence excitation time, which means that, at the moment of the fluorescence emission, any information about the initial absorption dipole orientation is lost. Assuming, furthermore, a uniform distribution of the orientations of the molecules' absorption dipoles, the observed fluorescence intensity will be proportional to

$$|T_p|^2 \langle S_+^{\text{obj}}/(S_+^{\text{tot}} + S_-)\rangle_{\hat{p}}, \tag{13}$$

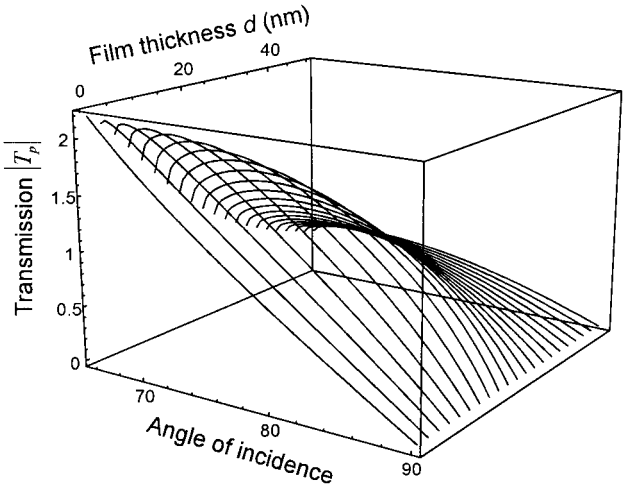

FIGURE 3 Dependence of the modulus of the transmission coefficient $|T_p|$ for a plane wave incident from the glass side onto the gold film upon the incidence angle θ_{inc} and the film thickness d at an excitation wavelength of $\lambda_{\text{ex}} = 514$ nm.

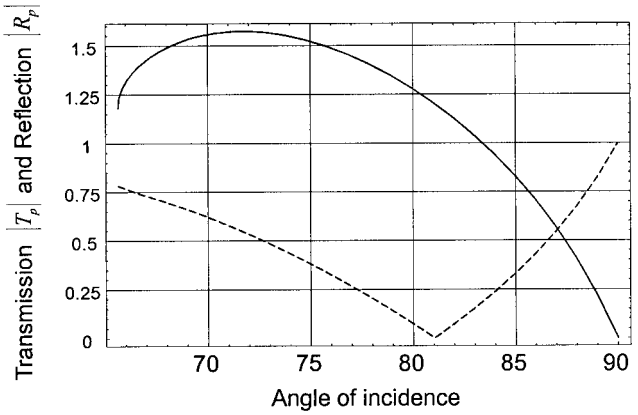

FIGURE 4 Modulus of the transmission (*solid line*) and reflection (*dashed line*) coefficients for the special case of gold film thickness $d = 19.79$ nm and excitation wavelength $\lambda_{\text{ex}} = 514$ nm.

where $\langle\ \rangle_{\hat{p}}$ refers to averaging over all possible emission dipole orientations. It should be noted that the last expression depends implicitly on the angle of incidence of the excitation light, the molecule's distance from the metal surface, and the thickness of the metal film.

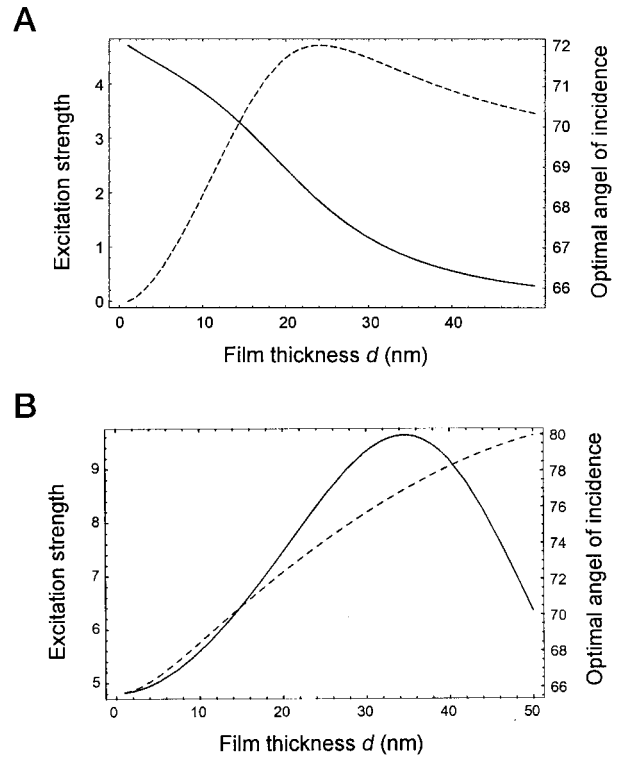

FIGURE 5 (*A*) Dependence of the optimal angle of incidence (*dashed line*) and the corresponding absolute square value of the transmission coefficient $|T_p^2|$ (*solid line*) upon gold film thickness at an excitation wavelength of 514 nm. (*B*) Same as (*A*), but for $\lambda_{\text{ex}} = 633$ nm.

RESULTS AND DISCUSSION

In this section, numerical results are presented for gold, silver, and aluminum films on glass (n_g = 1.46, quartz glass) covered with water (n_w = 1.33). Two different sets of excitation and emission wavelengths are studied: the excitation wavelength λ_{ex} = 514 nm and emission wavelength λ_{em} = 580 nm, corresponding to an argon ion laser exciting the dye TMR; and λ_{ex} = 633 nm and λ_{em} = 670 nm, corresponding to a diode laser exciting the dye Cy5. The complex refractive indices of the metals at these wavelengths were obtained from a Brendel–Bormann model as described in (Rakič et al., 1998). The values used are listed in Table 1.

First, we will consider the case of a thin gold film. Fig. 3 shows the dependence of the modulus of the transmission coefficient $|T_p|$ for a plane wave incident from the glass side onto the metal film upon the incidence angle θ_{inc} and the film thickness d at an excitation wavelength of λ_{ex} = 514 nm. Because we are only interested in an evanescent excitation of the fluorescence, the range of incidence angles studied starts with the angle of total internal reflection between glass and water (θ_0 = arcsin n_w/n_g = 65.64°) and ends at 90°. A film-thickness value of zero corresponds to a pure glass substrate covered with water, and, for that case, one sees the expected monotonically decreasing value of $|T_p|$ with increasing angle of incidence θ_{inc}. For a finite film thickness, this situation changes, and a maximum of the value of $|T_p|$ occurs at some intermediate angle between θ_0 and 90°. At that incidence angle, optical excitation of a molecule on the metal surface will be maximal (for a given film thickness). It should be noted that this optimal angle of incidence need not coincide with the angle of maximum excitation of surface plasmons. This is demonstrated in Fig. 4, showing the modulus of the transmission and reflection coefficients for the special case of d = 19.79 nm, a film thickness at which maximum efficiency of surface plasmon excitation is reached for λ_{ex} = 514 nm (reflectivity drops to zero). In that case, the optimal incidence angle for excitation lies near 72°, whereas minimal reflection (plasmon resonance) occurs at 81°.

For experimental applications, one is mainly interested in the optimal angle of incidence for excitation at a given film thickness. This corresponds to finding, at every value of film thickness, the maximum value of $|T_p|$ in Fig. 3. The result is shown in Fig. 5 *A*, where the dependence of this

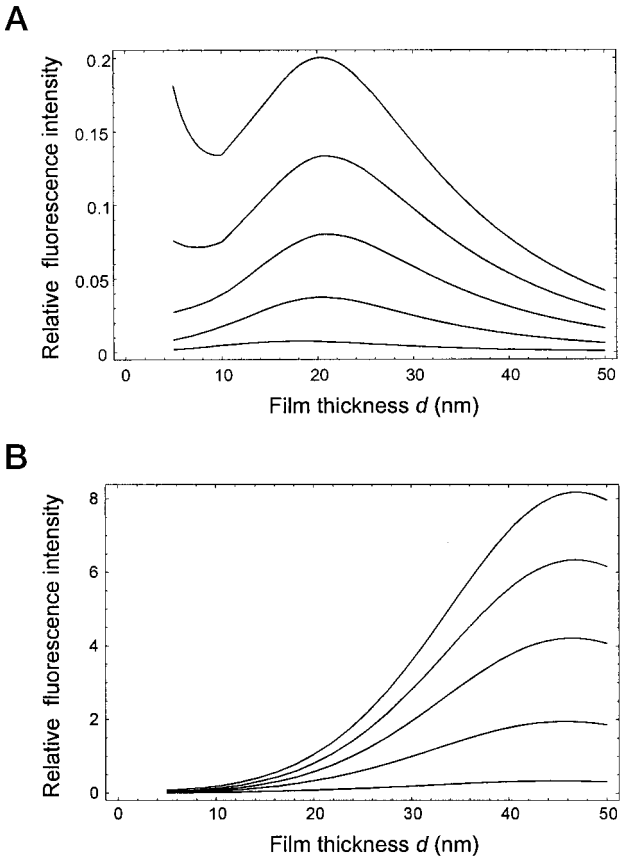

FIGURE 6 (*A*) Dependence of the normalized detectable fluorescence intensity upon gold film thickness. From the lowest curve through the highest, the molecule's distance changes from 5 nm through 25 nm in steps of 5 nm. The excitation wavelength was λ_{ex} = 514 nm, and the emission wavelength was λ_{em} = 580 nm. The incidence angle θ_{max} of excitation is always the optimal angle (see Fig. 5 *A*), for all values of film thickness. (*B*) Same as (*A*), but for λ_{ex} = 633 nm and λ_{em} = 670 nm.

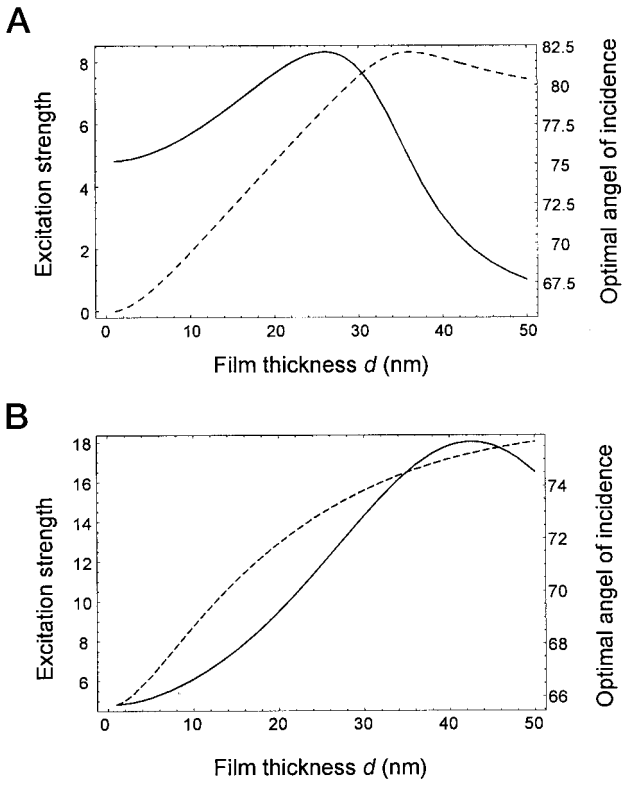

FIGURE 7 (*A*) Same as figure Fig. 5 *A* but for a silver film. (*B*) Same as figure Fig. 5 *B* but for a silver film.

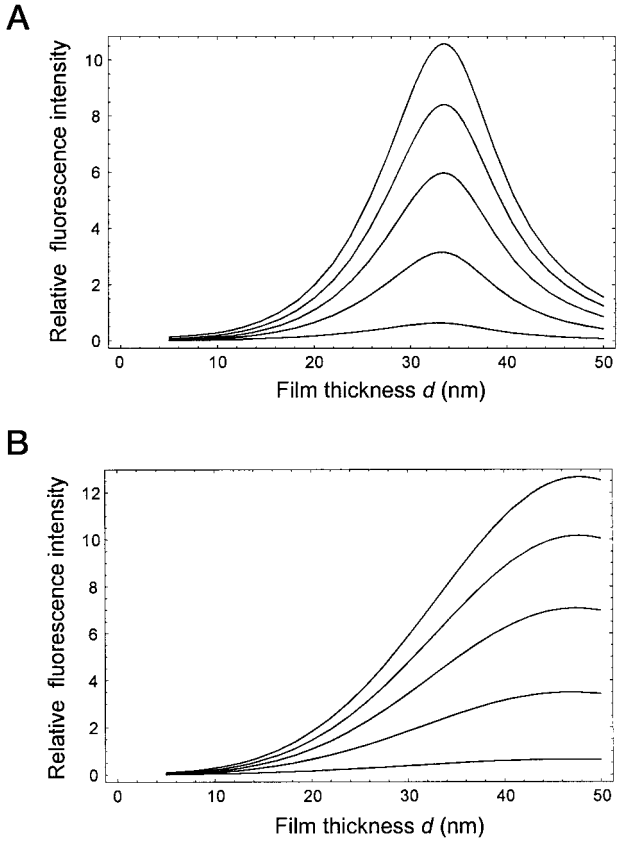

FIGURE 8 (*A*) Same as figure Fig. 6 *A* but for a silver film. (*B*) Same as figure Fig. 6 *B* but for a silver film.

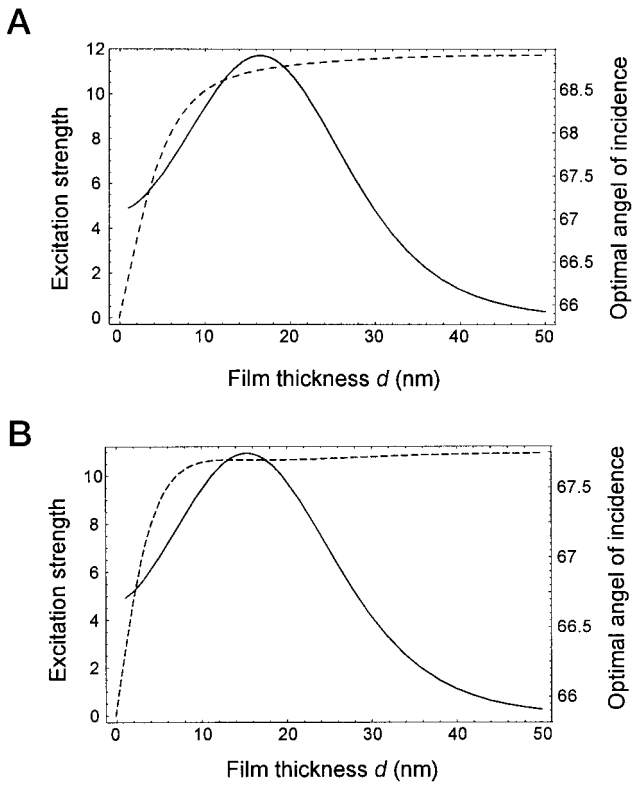

FIGURE 9 (*A*) Same as figure Fig. 5 *A* but for an aluminum film. (*B*) Same as figure Fig. 5 *B* but for an aluminum film.

optimal angle upon film thickness is shown, together with the corresponding factor $|T_p^2|$, which is directly proportional to the optical excitation rate of a molecule on the metal's surface. Figure 5 *B* shows the same dependence, but for an excitation wavelength of $\lambda_{ex} = 633$ nm. The large difference between Fig. 5, *A* and *B* is remarkable and a special effect of gold's peculiar dispersion relation.

Finally, the average fluorescence intensity was calculated at different distances of the molecule from the surface and for different values of film thickness according to Eq. 13, while assuming excitation at the optimal incidence angle (see Fig. 5). For comparison, the fluorescence intensity was always normalized by its value at zero film thickness (pure glass/water) but with the same excitation geometry and molecule position. Due to this normalization, we need not pay any attention to the exponential decrease of the electric field strength with increasing distance from the surface, because, at the same angle of incidence of the exciting light, this exponential factor is the same for any metal film thickness. The dependence of the normalized detectable fluorescence intensity, for the two pairs of excitation and emission wavelengths, on film thickness and on the molecule's distance from the surface are shown in Fig. 6, *A* and *B*. These figures show how much fluorescence intensity can be detected by the microscope objective at a given film thickness and molecule's distance under optimal excitation (maximal value of $|T_p^2|$) in comparison with the bare glass surface without metal film. Thus, Fig. 6, *A* and *B* can be directly used for optimally designing experimental conditions. If one would like, e.g., to perform an SMD experiment on a gold film at 514-nm excitation wavelength and fluorescence emission around 580 nm, Fig. 6 *A* gives the information that the optimal film thickness is 20 nm, and, for this film thickness, the optimal incidence angle for the excitation light is 71.5° (see Fig. 5 *A*). As can be also seen from Fig. 6 *A*, these optimal conditions are basically independent of the distance of the molecule from the metal film (of course, a larger distance increases the normalized fluorescence intensity, due to decreasing quenching). Moreover, if the molecule's distance is not completely fixed but can change with time, as will be the case for molecules linked to the surface by flexible linkers, than the normalized fluorescence intensity will be simply an average of the values shown by Fig. 6 *A*. If a molecule's distance fluctuates, e.g., between 20 and 25 nm, Fig. 6 *A* shows that the normalized fluorescence intensity will be between 0.14 and 0.2 (optimal conditions presumed, namely 20-nm film thickness and 71.5° incidence angle). Finally, a comparison of Fig. 6, *A* with *B* shows that, for gold films, the detectable fluorescence in-

tensity is much greater for the 633-nm excitation/670-nm emission case than for the 514-nm excitation/580-nm emission case, although under different optimal conditions (film thickness 45 nm and incidence angle 79°, see Fig. 5 *B* and Fig. 6 *B*).

These calculations have all been repeated for silver and aluminum films. In the following, only the dependence of the optimal angle of incidence and the corresponding transmission value upon film thickness are shown, together with the dependence of the normalized detectable fluorescence intensity on the film thickness and the molecule's position at optimal excitation. The results for silver films are shown in Fig. 7, *A* and *B* and Fig. 8, *A* and *B*; and the results for aluminum in Fig. 9, *A* and *B* and Fig. 10, *A* and *B*.

As can be seen by comparing Figs. 6 *A*, 8 *A*, and 10 *A*, at an excitation wavelength of 514 nm and emission wavelength of 580 nm, a silver film with film thickness near 34 nm will produce the highest detectable fluorescence intensity, at an excitation incidence angle of 86°. At an excitation wavelength of 633 nm and emission wavelength of 670 nm, silver gives still the best result, but at an increased film thickness near 48 nm and a reduced incidence angle near 75.5°. However, a gold film will yield comparably good results at these wavelengths.

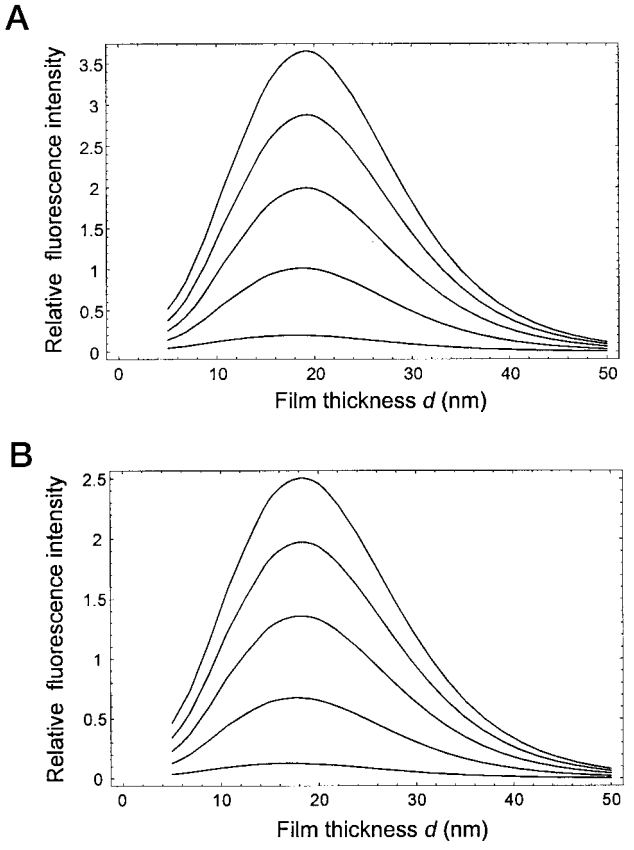

FIGURE 10 (*A*) Same as figure Fig. 6 *A* but for an aluminum film. (*B*) Same as figure Fig. 6 *B* but for an aluminum film.

TABLE 2 Comparison of relative fluorescence intensities as measured by Yokota et al. (1998) and as calculated in the present work.

	Source	
Metal	Yokota et al.	Present Work
Gold (20 nm)	1.57 ± 0.29	0.65
Silver (30 nm)	12.6 ± 2.6	9.6
Aluminum (30 nm)	2.33 ± 0.70	0.17

Incidence angle = 81°, numerical aperture of the microscope objective = 1.3, and the excitation and emission wavelengths are λ_{ex} = 514 nm and λ_{em} = 580 nm.

Finally, we will report a comparison between the values measured for TMR molecules by Yokota et al. (1998) with their set-up and our calculations. In their experiments, the angle of incidence was always the same and equal to 81°. They reported their measurements for an excitation wavelength of 514 nm and an emission wavelength centered around 580 nm (TMR). The fluorescing molecule was positioned nearly 25 nm away from the metal surface. The measured and calculated values are shown in Table 2. As can be seen, the correspondence between experimental and theoretical results is not excellent. There may be several reasons for this discrepancy. First, in the experiments, the TMR molecule was attached to a kinesin microtubule, and the distance of the TMR molecule was inferred from the diameter of these tubules (25 nm). Thus, the distance of the fluorescing molecule from the metal is not precisely known, which may lead to some improvement of the measurement/calculation correspondence if the real distance is larger than estimated. Second, and more seriously, in the present paper, all calculations were done for ideally flat metal films. It is a well-known fact that even slight corrugations of the film surface may lead to significant changes of the electrodynamic properties of the film (Pawley, 1995). In the work of Yokota et al. (1998), no information about surface properties of the used metal films were given. However, to include such film roughness effects into the calculations necessitates a much wider theoretical framework than that used in this paper, see, e.g., Parent et al. (1999).

I thank Martin Böhmer and Thomas Ruckstuhl for many inspiring discussions. I am grateful to Richard Ansell for his linguistic support. I would especially like to thank Eike Stedefeldt for his enduring and exceedingly helpful support of my work.

Support by the Volkswagenstiftung is gratefully acknowledged.

REFERENCES

Basché, T., W. E. Moerner, M. Orrit, and U. P. Wild, editors. 1997. Single Molecule Optical Detection, Imaging and Spectroscopy. VCH, Weinheim, Germany.

Born, M., and W. Wolf. 1989. Principles of Optics. Pergamon Press, Oxford, U.K.

Chance, R. R., A. Prock, and R. Silbey. 1978. Molecular fluorescence and energy transfer near interfaces. *Adv. Chem. Phys.* 37:1–65.

Enderlein, J., T. Ruckstuhl, and S. Seeger. 1999. Highly efficient optical detection of surface-generated fluorescence. *Appl. Opt.* 38:724–732.

Enderlein, J. 1999. Single molecule fluorescence near a metal layer. *Chem. Phys.* 247:1–9.

Girard, C., and A. Dereux. 1994. Optical spectroscopy of a surface at the nanometer scale: a theoretical study in real space. *Phys. Rev. B.* 49: 11344–11351.

Jackson, J. D. 1975. Classical Electrodynamics. John Wiley & Sons, New York.

Parent, G., D. Van Labeke, and D. Barchiesi. 1999. Fluorescence lifetime of a molecule near a corrugated interface: Application to near-field microscopy. *J. Opt. Soc. Am. A.* 16:896–908.

Pawley, J. B. 1995. Handbook of Biological Confocal Microscopy. Plenum Press, New York.

Rakič, A. D., A. B. Djurišič, J. M. Elazar, and M. L. Majewski. 1998. Optical properties of metallic films for vertical-cavity optoelectronic devices. *Appl. Opt.* 37:5271–5283.

Yokota, H., K. Saito, and T. Yanagida. 1998. Single molecule imaging of fluorescently labeled proteins on metal by surface plasmons in aqueous solution. *Phys. Rev. Lett.* 80:4606–4609.